Journal of Solid State Chemistry 182 (2009) 1142–1148

Contents lists available at ScienceDirect

Journal of Solid State Chemistry

journal homepage: www.elsevier.com/locate/jssc

Phase equilibria and crystal chemistry of the *R*–Cu–Ti–O systems (*R* = lanthanides and Y)

Z. Yang [a], W. Wong-Ng [d,*], J.A. Kaduk [b], M. Jang [c], G. Liu [d]

[a] Yunnan Normal University, Kunming 650092, PR China
[b] INEOS Technologies, Naperville, IL 60563, USA
[c] Yonsei University, Seoul 120–740, Korea
[d] Ceramics Division, National Institute of Standards and Technology, Giathersburg, MD 20899, USA

ARTICLE INFO

Article history:
Received 25 June 2008
Received in revised form
4 November 2008
Accepted 11 November 2008
Available online 21 November 2008

Keywords:
R–Cu–Ti–O (*R* = lanthanides)
Coated conductors
Phase equilibria
Crystal chemistry
Reference X-ray powder patterns

ABSTRACT

As part of the study of interaction of the $Ba_2RCu_3O_{6+z}$ (*R* = lanthanides and Y) superconductor with $SrTiO_3$ buffer, phase equilibria of the subsystem, R_2O_3–TiO_2–CuO (*R* = Nd, Y, and Yb), have been investigated in air at 960 °C. While the phase relationships of the two phase diagrams with smaller *R* (Y and Yb) are similar, substantial differences were found in the Nd_2O_3–TiO_2–CuO system, partly due to different phase formation in the binary R_2O_3–TiO_2 and R_2O_3–CuO systems. R_2CuTiO_6 and $R_2Cu_9Ti_{12}O_{36}$ were the only ternary phases established in all the three diagrams. $R_2Cu_9Ti_{12}O_{36}$ belongs to the perovskite-related $[AC_3](B_4)O_{12}$ family which is cubic *Im*3. Depending on the size of R^{3+}, R_2CuTiO_6 crystallizes in two crystal systems: *Pnma* (*R* = La–Gd), and $P6_3cm$ (*R* = Dy–Lu). The structure and crystal chemistry of the *Pnma* series of R_2CuTiO_6 (*R* = La, Nd, Sm, Eu, and Gd) are discussed in detail in this paper. Patterns for selected members of R_2CuTiO_6 have also been prepared and submitted for inclusion in the Powder Diffraction File (PDF).

Published by Elsevier Inc.

1. Introduction

With increasing global utilization of electricity in recent years, energy shortages and electricity outages have become common problems. Consequently, there are pressing needs for improvements in electrical distribution grids and for more efficient utilization of energy resources. High temperature superconductors have demonstrated potential for meeting these needs [1]. There is continued effort within the high T_c community on research and development of coated conductors for wire and tape applications [2–7]. These coated conductors are based on $Ba_2YCu_3O_x$ (Y-213) and $Ba_2RCu_3O_x$ (*R*-213, *R* = lanthanides) as the principal superconductors. Y-213 and *R*-213 can be deposited on flexible substrates using various techniques [8–14], and the resulting tapes show excellent current carrying capability.

State-of-the-art substrates and buffer layers form the basis for coated conductor fabrication. Despite many benefits of the use of buffer layers, including the promotion of epitaxial growth of $Ba_2YCu_3O_{6+x}$, there are unavoidable reactions at the interfaces between the layers [15,16]. Understanding of interfacial reactions of Y-213/*R*-213 phases with the buffer layers will provide information about how to avoid and/or control the formation of secondary phases. Phase equilibrium data will also assist interpretation of the results of transmission electron microscopy (TEM) analysis of coated conductor interfaces.

$SrTiO_3$ is one of the possible buffer layer materials for the ion beam assisted deposition (IBAD) technique [2,3], which has been largely developed at Los Alamos National Laboratory. $SrTiO_3$ is also one of the model substrates for studying phase formation mechanism [8,17–20]. As part of our studies of the interaction of $Ba_2YCu_3O_{6+z}$ with $SrTiO_3$, we report the crystal chemistry and phase equilibria of the R_2O_3–TiO_2–CuO (*R* = Nd, Y, and Yb) subsystems as well as the characterization of the ternary series, R_2CuTiO_6 (*R* = Nd, Sm, Eu, and Gd). Since reference X-ray powder diffraction patterns are important for phase characterization, we have also prepared selected patterns in the *R*–Cu–Ti–O systems for inclusion in the Powder Diffraction File (PDF) [21].

2. Experimental[1]

Compounds within the *R*–Ti–Cu–O (*R* = Nd, Y, and Yb) systems were prepared by heating a stoichiometirc mixture of CuO, R_2O_3, and TiO_2 in air. R_2O_3 were first heat-treated at 850 °C overnight

* Corresponding author. Fax: +1 301 975 5334.
E-mail address: Winnie.wong-ng@nist.gov (W. Wong-Ng).

[1] The purpose of identifying the equipment in this article is to specify the experimental procedure. Such identification does not imply recommendation or endorsement by the National Institute of Standards and Technology.

0022-4596/$ - see front matter Published by Elsevier Inc.
doi:10.1016/j.jssc.2008.11.010

Table 1
Compositions (#1–23) prepared for the phase diagram study of the R_2O_3–TiO_2–CuO (R = Nd, Y, and Yb) systems and three additional compositions (#24–26) prepared for the Nd_2O_3–TiO_2–CuO system.

#	TiO_2	$1/2R_2O_3$	CuO
1	25	50	25
2	52.1	8.7	39.2
3	25	65	10
4	10	70	20
5	10	55	35
6	10	30	60
7	20	30	50
8	35	45	20
9	30	15	55
10	45	35	20
11	55	35	10
12	35	55	10
13	90	5	5
14	65	15	20
15	67	3	30
16	30	2	68
17	0	66.7	33.3
18	0	50	50
19	33.3	66.7	0
20	50	50	0
21	60	40	0
22	70	0	30
23	40	0	60
24	65	30	5 (R = Nd)
25	75	20	5 (R = Nd)
26	60	40	0 (R = Nd)

The compositions are expressed in mol fraction, %.

prior to use. Samples were weighed out, well-mixed and calcined at 950 °C for 1 day and at 960–970 °C for about 15 days with intermediate grindings. For phase equilibrium studies, a total of 26, 23, and 23 samples were prepared for the R = Nd, Y and Yb systems (Table 1), respectively. In addition to the phase diagram study, we have also investigated the crystal chemistry and crystallography of the R_2CuTiO_6 series (R = La, Nd, Sm, Eu, and Gd). Solid state sample preparation techniques as described above were applied, with the highest temperature of heat-treatment at 1050–1100 °C for a total of 2 weeks. The purity of the samples was confirmed by powder X-ray diffraction.

During reference pattern determination for R_2CuTiO_6, the powders were deposited on zero-background cells as acetone slurries. The specimens were rotated during the measurements of the powder patterns. The patterns were measured on a Bruker D8 advanced diffractometer equipped with a VÅNTEC-1 position-sensitive detector. The patterns were measured (Cu$K\alpha$ radiation, 40 kV, 40 mA, 0.3° divergence slit) from 5° to 150° 2θ in 19871 steps, counting for 0.5 or 1 s per step. The structure of R_2CuTiO_6 was determined using the Rietveld refinement technique [22] with the software suite GSAS [23]. Reference patterns were obtained with a Rietveld pattern decomposition technique. In this technique, the reported peak positions are derived from the extracted integrated intensities and positions calculated from the lattice parameters. When peaks are not resolved at the resolution function characteristics of a good laboratory diffractometer, the intensities are summed, and an intensity-weighted d-spacing is reported. Therefore, these patterns represent ideal specimen patterns. They are corrected for systematic errors both in d-spacing and intensity.

3. Results and discussion

A phase diagram of the Nd_2O_3–CuO–TiO_2 system is shown in Fig. 1. Figs. 2 and 3 give the phase diagrams for R_2O_3–CuO–TiO_2 systems with R = Y and Yb. These two diagrams are similar to each other. Phase compatibility of these R_2O_3–CuO–TiO_2 systems, and a comparison with that of the La-analog [24] will be discussed in the following sections. Crystal chemistry and crystallography of R_2CuTiO_6 and $R_2Cu_9Ti_{12}O_{36}$ will also be described. The reported lattice parameters in this paper including those taken from literature were measured at ambient conditions.

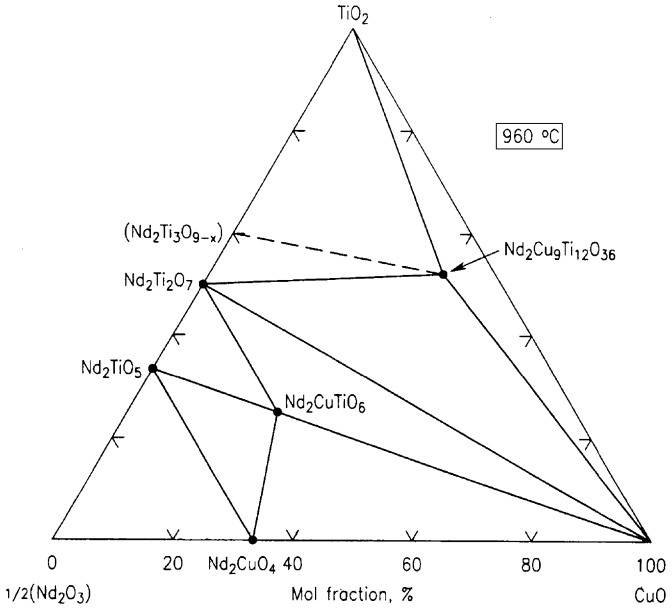

Fig. 1. Phase diagram of the Nd_2O_3–CuO–TiO_2 system prepared in air at 960 °C.

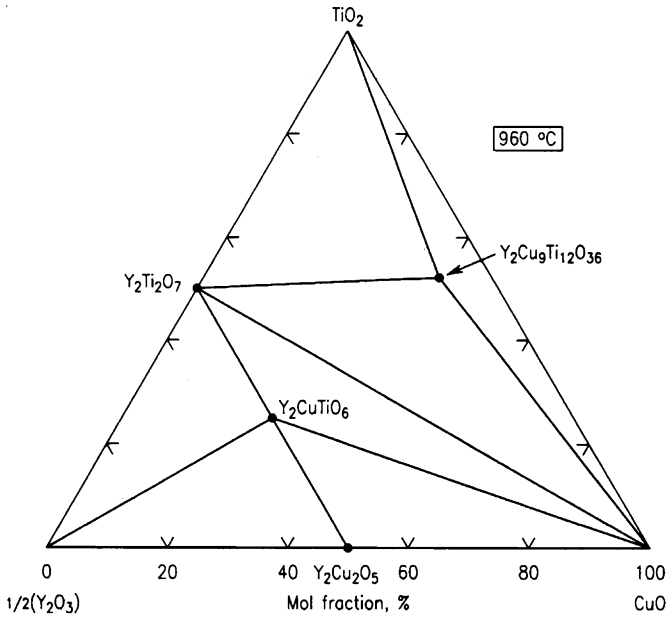

Fig. 2. Phase diagram of the Y_2O_3–CuO–TiO_2 system prepared in air at 960 °C.

3.1. Phase diagrams of the R_2O_3–CuO–TiO_2 systems (R = Nd, Y, and Yb)

In the R_2O_3–CuO systems, only one binary oxide phase was confirmed. Depending on the size of R the binary phase is

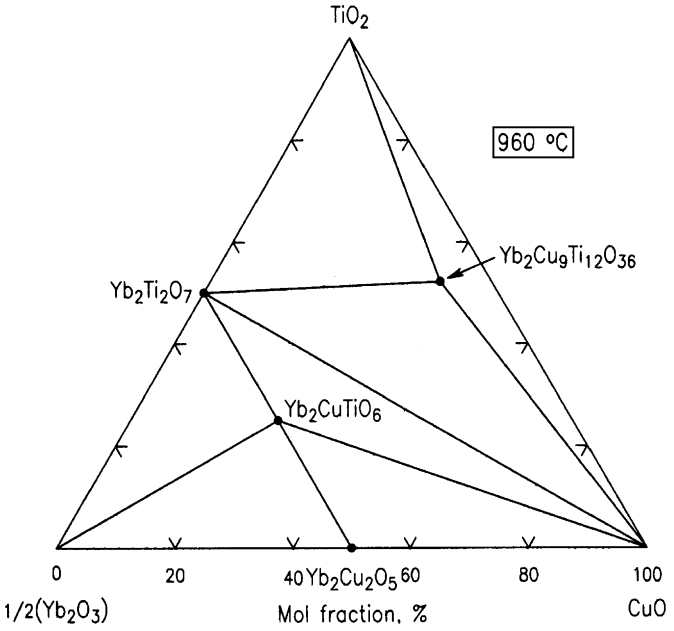

Fig. 3. Phase diagram of the Yb_2O_3–CuO–TiO_2 system prepared in air at 960 °C.

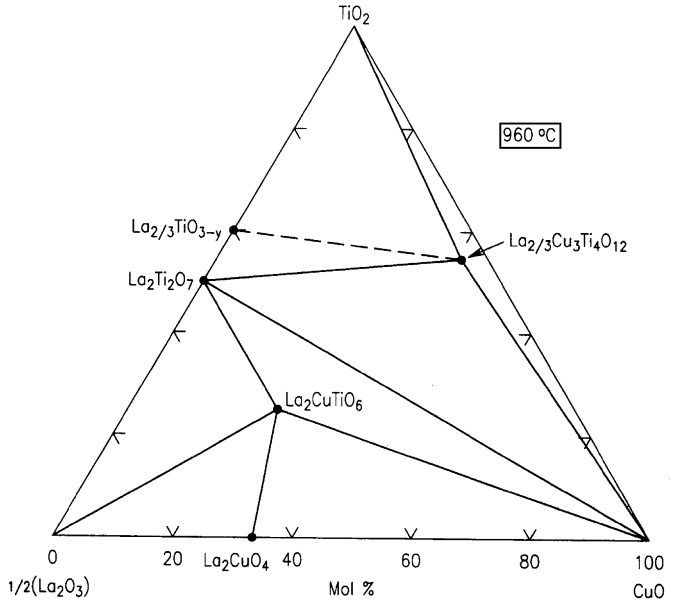

Fig. 4. Phase diagram of the La_2O_3–CuO–TiO_2 system prepared in air at 960 °C.

different, namely, R_2CuO_4 (R = Nd) vs. $R_2Cu_2O_5$ (R = Y and Yb). Nd_2CuO_4 crystallizes in the space group of I4/*mmm*, $a = 3.937$ Å and $c = 12.155$ Å (PDF 24-777) [21]; $Y_2Cu_2O_5$ belongs to the orthorhombic system *Pna*2$_1$, $a = 10.8003(8)$ Å, $b = 3.4953(8)$ Å, and $c = 12.4588(8)$ Å (PDF 1-78-2100). The cell parameters for $Yb_2Cu_2O_5$ are $a = 10.7290(1)$ Å, $b = 3.4355(1)$ Å, and $c = 12.3531(1)$ Å (PDF 4-006-8559).

Two phases were determined in the TiO_2–Nd_2O_3 system: $Nd_2Ti_2O_7$ (*P*2$_1$, $a = 13.008(2)$ Å, $b = 5.4648(7)$ Å, $c = 7.679(2)$ Å, $\beta = 98.56\ (2)^\circ$ (PDF 33-942)), and Nd_2TiO_5 (*Pnam*, $a = 10.7251(9)$ Å, $b = 11.3407(10)$ Å, and $c = 3.8457(4)$ Å (PDF 33-944)). However, in the TiO_2–Y_2O_3 and TiO_2–Yb_2O_3 systems, only the $R_2Ti_2O_7$ phase (*Fd*-3*m*, R = Y, $a = 10.0950(5)$ Å (PDF 1-73-1697); R = Yb, $a = 10.030$ Å (PDF 17-454)) was found.

In agreement with the study by Anderson et al. [24], no compound was found in the TiO_2–CuO system under the current experimental conditions. The phases that were reported in literature, namely, Cu_3TiO_5 [25], Cu_3TiO_4 [26], and $Cu_2Ti_4O_x$ [27] were stable only at temperatures above 1000 °C. The $Cu_3Ti_3O_x$ phase can only be prepared under inert atmosphere [28].

Two ternary phases were determined in the R_2O_3–CuO–TiO_2 systems, namely, R_2CuTiO_6 and $R_2Cu_9Ti_{12}O_{36}$. Tie–line relationships near the CuO corner are the same in all three diagrams, but significant differences were found in the R_2O_3 and TiO_2-rich regions, mainly due to different phases formed in the TiO_2–R_2O_3 and R_2O_3–CuO systems. While there is a compatibility line between R_2CuTiO_6 and R_2O_3 (R = Y and Yb), this tie–line does not exist in the R = Nd system; instead a tie–line between Nd_2TiO_5 and Nd_2CuO_4 was found. In the Ti-rich region, a single phase, $Nd_2Ti_3O_{9-x}$, has been reported by Richard et al. [29] using solution synthesis approach at a relatively low temperature; however, it could not be prepared under the current processing condition, as it contains $Nd_2Ti_2O_7$. Single-phase $La_2Ti_3O_{9-x}$ was reported to be an A-site and oxygen deficient perovskite which exhibits both a cubic (when x is large), and an orthorhombic structure (when x is small) [24,30].

Comparing the three R_2O_3–CuO–TiO_2 (R = Nd, Y, and Yb) phase diagrams with the La-analog (Fig. 4) [24], a trend of phase formation can be established. For example, the binary $R_2Ti_2O_7$ phase and the ternary $R_2Cu_9Ti_{12}O_{36}$ and R_2CuTiO_6 phases were found in all four systems. In the larger R = La and Nd-systems, two binary R–Ti–O phases were found ($La_2Ti_2O_7$ and $La_2Ti_3O_{9-x}$ in the La-system vs. $Nd_2Ti_2O_7$ and R_2TiO_5 in the Nd-system), while only one binary oxide phase exists in the systems with smaller size of R^{3+}.

3.2. Structure of $R_2Cu_9Ti_{12}O_{36}$

This series of compounds has received considerable interest in recent years because of their high dielectric constants [31–34]. The details of the structure of $R_2Cu_9Ti_{12}O_{36}$ have been reported previously from this laboratory [35]. In brief, $R_2Cu_9Ti_{12}O_{36}$ belong to the perovskite-related $[AC_3](B_4)O_{12}$ family, are cubic with space group *Im*3 [36] and are isostructural to $Bi_{2/3}Cu_3Ti_4O_{12}$ [37]. The lattice parameters for the eleven $R_2Cu_9Ti_{12}O_{36}$ (R = Nd, Sm, Eu, Gd, Dy, Ho, Y, Er, Tm, Yb, and Lu) phases span a range of 7.39987(3)–7.37757(2)Å, and the unit cell volume, V, from 405.202(4) to 401.550(3) Å^3 [35]. The doubling of the unit cell as compared to the simple ABO_3 type is the result of the ordering between the A and C cations in the $[AC_3](B_4)O_{12}$ family [38]. The structure of $R_2Cu_9Ti_{12}O_{36}$ (Fig. 5) can be considered as consisting of three types of polyhedra: R occupies the larger icosahedral A site of the ideal ABO_3 perovskite structure, while Ti occupies the distorted octahedral B site. The Jahn–Teller cation Cu occupies the C site. The 12 oxygens surrounding Cu are arranged as three mutually perpendicular rectangles of different size. The smallest and largest rectangles are nearly squares. One-third of the R site is vacant; therefore, the chemical formula can be written as $[R_{2/3}X_{1/3}Cu_3](Ti_4)O_{12}$, where X = vacancy.

3.3. Structure of R_2CuTiO_6

Table 2 gives the refinement residuals using the Reitveld refinement technique. Fig. 6 shows the observed (crosses) and calculated (solid line) X-ray intensities pattern for Eu_2TiCuO_6 at 295 K. Differences in intensity between the observed and calculated patterns are shown at the bottom of the figure. Vertical

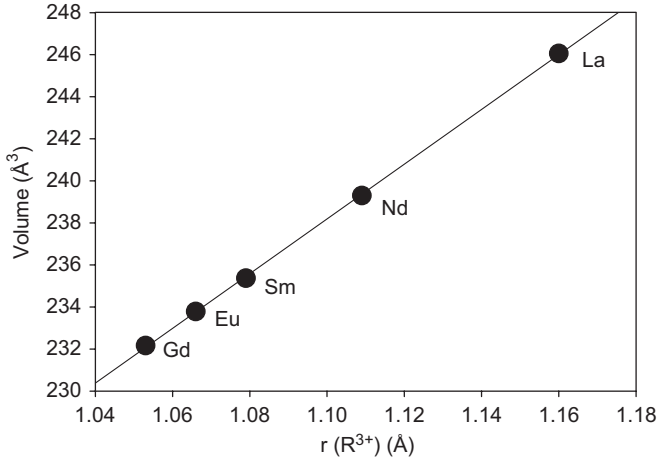

Fig. 5. Cell volume of R_2TiCuO_6 showing a monotonic decreasing trend as a function of the Shannon ionic radius of r (R^{3+}) [41–42].

Table 2
R_2TiCuO_6 refinement residuals.

R	Nd	Sm	Eu	Gd
wRp	0.0729	0.0356	0.0321	0.0179
Rp	0.0567	0.0276	0.0248	0.0140
χ^2	1.395	1.405	1.381	1.349
$R(F)$	0.0605	0.0618	0.0616	0.0863
$R(F^2)$	0.0999	0.1007	0.0947	0.1188
ΔF (e/Å^3)	2.66	2.01	2.37	3.67
	−2.62	−2.26	−2.81	−3.26
#Variables	26	28	27	25
#Observations	17813	18635	17813	17828

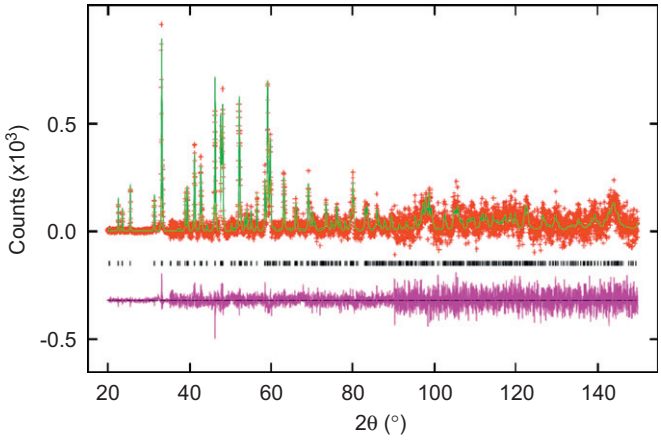

Fig. 6. Observed (crosses) and calculated (solid line) X-ray intensities pattern for $Ba(Nd_{0.8}Y_{1.2})CuO_5$ at 295 K. Differences in intensity between the observed and calculated patterns are shown at the bottom of the figure. Vertical lines indicate the Bragg positions.

Table 3
Lattice parameters for R_2TiCuO_6 (R = Nd, Sm, Eu, and Gd).

R	r(R^{3+}) (Å)	a (Å)	b (Å)	c (Å)	V (Å^3)
La [24]	1.160	5.616 (5)	7.842 (7)	5.587 (6)	246.06
Nd	1.109	5.7247 (3)	7.6350 (3)	5.4750 (3)	239.30 (2)
Sm	1.079	5.74812 (11)	7.56025 (14)	5.41621 (10)	235.373 (10)
Eu	1.066	5.75444 (10)	7.54182 (14)	5.38684 (10)	233.783 (10)
Gd	1.053	5.75742 (9)	7.52298 (12)	5.36018 (9)	232.165 (8)

Space group: *Pnma*; r (R^{3+}) is the Shannon ionic radius taken from Refs. [41,42].

Table 4
Atomic coordinates of R_2TiCuO_6 (R = Nd, Sm, Eu, and Gd).

R	x	Y	z	Occ	U_{iso} (Å^2)	M
(1) Nd_2TiCuO_6						
Nd_1	0.5578 (2)	0.25	0.0104 (5)	1.0	0.0130 (5)	4
Ti_2/Cu_3	0.0	0.0	0.0	0.5	0.0017 (9)	4
O_4	0.246 (3)	0.031 (2)	0.170 (2)	1.0	0.022 (4)	8
O_5	0.971 (2)	0.25	0.899 (3)	1.0	0.022 (4)	4
(2) Sm2TiCuO6						
Sm1	0.5654 (2)	0.25	0.0166 (3)	1.0	0.0168 (4)	4
Ti_2/Cu_3	0.0	0.0	0.0	0.5	0.0074 (7)	4
O_4	0.278 (2)	0.0451 (13)	0.201 (2)	1.0	0.058 (3)	8
O_5	0.976 (2)	0.25	0.884 (2)	1.0	0.058 (3)	4
(3) Eu_2TiCuO_6						
Eu_1	0.5695 (2)	0.25	0.0166 (3)	1.0	0.0138 (4)	4
Ti_2/Cu_3	0.0	0.0	0.0	0.5	0.0089 (7)	4
O_4	0.2865 (15)	0.0512 (10)	0.202 (2)	1.0	0.028 (2)	8
O_5	0.974 (2)	0.25	0.877 (2)	1.0	0.028 (2)	4
(4) Gd_2TiCuO_6						
Gd_1	0.57275 (13)	0.25	0.0175 (3)	1.0	0.0187 (4)	4
Ti_2/Cu_3	0.0	0.0	0.0	0.5	0.0081 (6)	4
O_4	0.2811 (12)	0.0534 (8)	0.1893 (12)	1.0	0.038 (2)	8
O_5	−0.0292 (15)	0.25	−0.1220 (14)	1.0	0.038 (2)	4

Occ stands for site occupancy; U_{iso} stands for isotropic displacement factor, and M is multiplicity

lines indicate the Bragg positions. Table 3–5 give the lattice parameters, atomic coordinates with isotropic displacement factors, and bond distances, respectively.

Anderson et al. [39] gave a detailed review of the B-cation arrangements in the A′A″B′B′O$_6$ double perovskites, including the R_2TiCuO_6 series. In summary, four factors that determine the B-cation arrangement in A′A″B′B′O$_6$ perovskites are differences in charge, ionic radius, cation coordination geometry, and the A-cation/B-cation size ratio. The B-cations may order in a random, rock salt, or layered fashion. Among the five common systems observed in these materials, the randomly distributed B-cation sublattices with BO_6 octahedra tilting usually has an orthorhombic *Pbnm* ($\sqrt{2}a_p \times \sqrt{2}a_p \times 2a_p$) structure. An orthorhombic cell is observed when the A–O bond length is less than $\sqrt{2}$ times the B–O bond length, or the Goldschmidt tolerance factor, $t<1$ [40]. Depending on the size of R^{3+} [41,42], two structure types of R_2TiCuO_6 were reported, namely orthorhombic *Pnma* (R = La, Nd, Sm, Eu, and Gd), and hexagonal $P6_3cm$ (R = Dy, Ho, Er, Tm, Yb, and Lu) [24,43]. The structure of the hexagonal members, with R = Y, Tb–Lu, has been reported [43].

R_2TiCuO_6 (R = La, Nd, Sm, Eu, and Gd) are isostructural to $GdFeO_3$ [44]. R resides in an eight-membered cage, while Ti and Cu are disordered inside octahedral cages. Fig. 7 and Table 3 show the monotonic decrease of the lattice parameters as a function of the lanthanide contraction. It is interesting to see that as the size of R^{3+} decreases, the cell dimensions b and c decrease, as expected; however, the corresponding value for a increases. As seen in Fig. 8 of the structure, the BO_6 octahedra rotate about $[011]_{cubic}$ and the $[100]_{cubic}$ ($a^-b^-b^-$ in Glazer's rotation [45]). These octahedra tilt to optimize eight of the originally equal 12 A–O bond distances [39]. Apparently, this optimization gives rise to the different trend of the cell parameters a, b, and c.

Table 5 gives the lengths of the relevant bonds and the bond valence sum values (BVS) [46,47] for R, Cu and Ti. The bond

Table 5
Bond distances (Å) in R_2TiCuO_6 (R = Nd, Sm, Eu, and Gd).

Atoms	Bond distance	BVS	Atoms	Bond distance	BVS		
					Ti	Cu	Cu/Ti
(1) Nd_2TiCuO_6							
Nd_1–O_4	2.598 (14) × 2	2.57	Ti_2/Cu_3–O_4	1.702 (12) × 2	4.44	3.07	3.76
	2.615 (15) × 2			2.334 (11) × 2			
	2.65 (2) × 2			1.994 (5) × 2			
Nd_1–O_5	2.441 (12) × 1						
	2.30 (2) × 1						
(2) Sm_2TiCuO_6							
Sm_1–O_4	2.477 (10) × 2	2.81	Ti_2/Cu_3–O_4	1.961 (12) × 2	3.52	2.44	2.98
	2.680 (10) × 2			2.092 (11) × 2			
	2.495 (10) × 2			1.997 (3) × 2			
Sm_1–O_5	2.466 (10) × 1						
	2.230 (10) × 1						
(3) Eu_2TiCuO_6							
Eu_1–O_4	2.429 (8) × 2	2.94	Ti_2/Cu_3–O_4	2.012 (9) × 2	3.41	2.36	2.88
	2.689 (8) × 2			2.059 (9) × 2			
	2.471 (8) × 2			2.004 (3) × 2			
Eu_1–O_5	2.445 (11) × 1						
	2.192 (10) × 1						
(4) Gd_2TiCuO_6							
Gd_1–O_4	2.420 (6) × 2	2.91	Ti_2/Cu_3–O_4	1.952 (7) × 2	3.46	2.40	2.93
	2.673 (6) × 2			2.127 (7) × 2			
	2.469 (7) × 2			1.998 (2) × 2			
Gd_1–O_5	2.410 (9) × 1						
	2.200 (8) × 1						

Since the Cu/Ti sites are mixed (in 50:50 ratio), for comparison purpose, three bond valence sum (BVS) values [46,47] were computed by assuming that the sites are occupied by Cu, Ti, and mixed Cu/Ti.

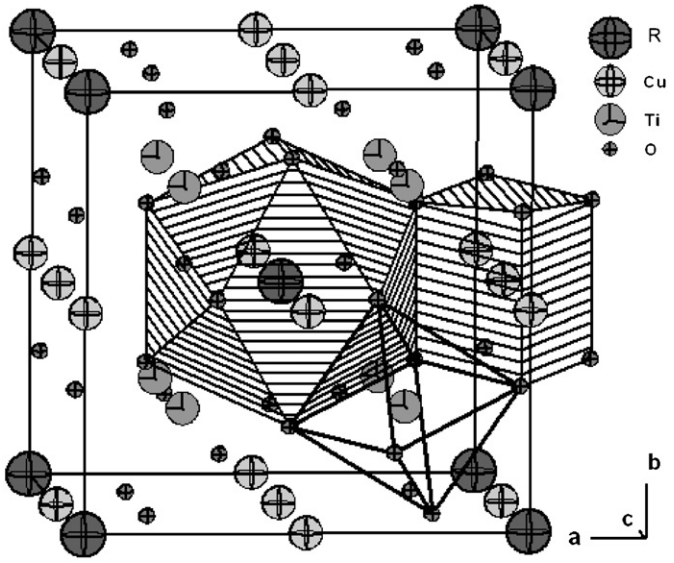

Fig. 7. Crystal structure of $R_2Cu_9Ti_{12}O_{36}$ [35,36].

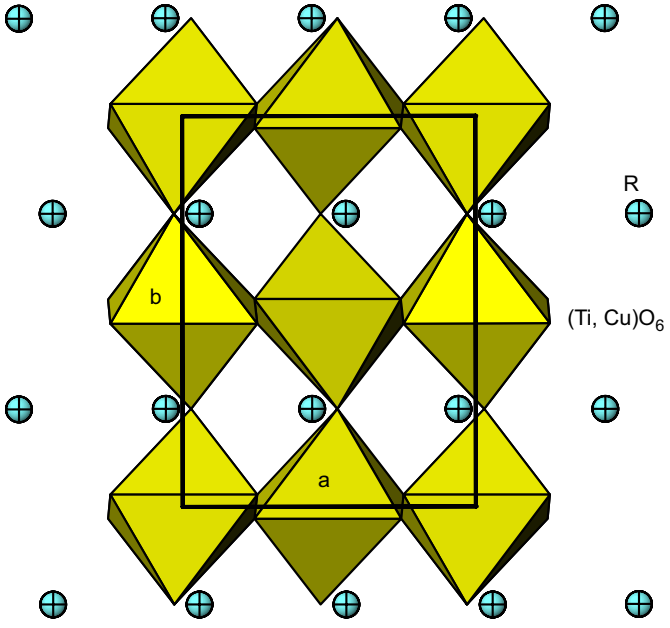

Fig. 8. Crystal structure of R_2TiCuO_6, where R = Nd, Sm, Eu, and Gd, featuring the tilting of the Ti/CuO_6 octahedra.

valence values used for Cu–O and Ti–O are 1.679 and 1.815, and those for Nd–O, Sm–O, Eu–O, and Gd–O are 2.117, 2.088, 2.076, and 2.065, respectively [46,47]. For the Cu/Ti sites, we report BVS calculations for assuming full site occupancy for Ti, for Cu, and for 50:50 mole ratios of Ti/Cu. One can in general consider the BVS as an indication for the strain state of the cations in a cage. A value that is larger than the ideal valence is considered as compressive strain, or the cage in which the cation resides is too

small. On the other hand, a small value suggests tensile strain, or the cage is too large. At a glance, in the present case, Nd_2TiCuO_6 experiences most strain: with the smallest BVS (2.57) for 'Nd' in the eight-membered Nd–O cage and the largest value for Ti/Cu (3.76) in the octahedral cage. As the ionic size of the lanthanide cation decreases, both compressive and tensile strain relax, and the BVS values for Eu and Gd approach that of the ideal valence of '3', and that of Ti/Cu approaches the ideal average value of '3' as well (a mean value between a Ti^{4+} cation and a Cu^{2+} cation of the mixed site).

3.4. Powder diffraction patterns for R_2CuTiO_6

Powder diffraction patterns for $R_2Cu_9Ti_{12}O_{36}$ have been submitted and published in the PDF and will not be reported in this paper. Preparation of X-ray powder reference patterns for R_2TiCuO_6 (R = Nd, Sm, Eu, Gd, Dy, Ho, Er, Tm, Yb, Lu, and Y) have been completed and have been submitted to the International Centre for Diffraction Data (ICDD) to be included in the PDF. Tables 6 and 7 give two examples of experimental patterns of R_2TiCuO_6: R = Sm (*Pnma*) and R = Y phases ($P6_3cm$). In these tables, the symbols *M* and + refer to peaks containing contributions from two and more than two reflections, respectively. The symbol * indicates the particular peak that has the strongest intensity of the entire pattern and is designated a value of '999'. The intensity values reported are integrated intensities rather than peak heights.

3.5. Summary

The phase equilibrium study of the R_2O_3–TiO_2–CuO (R = Nd, Y, and Yb) systems gives a trend of phase formation as a function of the ionic radius of R^{3+}. While the diagrams for R = Y and Yb are similar, they are different from that of the R = La and Nd systems, particularly in the CuO-poor region. Crystal chemistry and X-ray patterns of selected R_2TiCuO_6 phases have been studied and prepared, respectively.

Table 6
X-ray reference pattern for Sm_2TiCuO_6, *Pnma* (no. 62), $a = 5.74812(11)$ Å, $b = 7.56025(14)$ Å, $c = 5.41621(10)$ Å, $V = 235.373(10)$ Å^3.

d (Å)	I	h	k	l	d (Å)	I	h	k	L	d (Å)	I	h	k	l
4.4029	6	0	1	1	3.9420	130	1	0	1	3.7801	84	0	2	0
3.4954	167	1	1	1	2.8741	177	2	0	0	2.7284	999*	1	2	1
2.7081	235	0	0	2	2.6865	127	2	1	0	2.5388	5	2	0	1
2.3305	35	1	1	2	2.2879	50	2	2	0	2.2015	94	0	2	2
2.1233	67	1	3	1	2.1076	5	2	2	1	1.9710	166	2	0	2
1.9072	119	2	1	2	1.8948	74	2	3	0	1.8901	148	0	4	0
1.7569	171	3	1	1*M*	1.7569	171	1	3	2*M*	1.7477	8	2	2	2
1.7224	17	1	0	3	1.7043	35	1	4	1	1.6794	28	1	1	3
1.6298	66	3	2	1	1.5792	89	2	4	0	1.5674	208	1	2	3
1.5525	49	2	3	2	1.5499	100	0	4	2	1.4985	13	2	1	3
1.4681	98	3	3	1*M*	1.4681	98	0	3	3*M*	1.4370	7	4	0	0
1.4220	8	1	3	3	1.4118	56	1	5	1*M*	1.4118	56	4	1	0*M*
1.3890	6	4	0	1	1.3642	96	2	4	2	1.3541	27	0	0	4
1.3432	7	4	2	0	1.3382	14	2	5	0	1.2984	10	1	1	4
1.2946	43	3	1	3	1.2747	7	0	2	4	1.2731	19	1	4	3
1.2600	7	0	6	0	1.2519	45	4	1	2	1.2483	20	4	3	0
1.2411	21	3	2	3	1.2249	22	2	0	4	1.2092	22	2	1	4
1.2034	7	4	2	2	1.2001	97	1	6	1*M*	1.2001	97	2	5	2*M*
1.1679	6	1	3	4	1.1651	34	3	3	3	1.1594	43	3	5	1
1.1424	6	0	6	2	1.1363	8	1	5	3	1.1337	41	4	3	2
1.1246	15	5	0	1	1.1123	30	5	1	1	1.1017	17	2	3	4
1.1007	31	0	4	4	1.0777	6	4	2	3	1.0613	5	3	2	4
1.0417	22	4	5	0*M*	1.0417	22	1	7	1*M*	1.0334	13	3	6	1
1.0279	25	2	4	4	1.0270	21	5	3	1	1.0247	40	1	2	5
1.0170	45	1	6	3	1.0110	7	2	7	0	0.9918	19	3	5	3
0.9772	22	4	1	4	0.9722	23	4	5	2	0.9697	9	5	0	3
0.9664	19	5	4	1	0.9618	16	5	1	3	0.9536	6	4	2	4
0.9518	13	2	5	4	0.9504	5	6	1	0	0.9472	16	2	7	2
0.9450	15	0	8	0	0.9357	17	3	1	5	0.9287	23	6	2	0
0.9275	6	1	4	5	0.9270	29	3	7	1	0.9190	8	1	8	1
0.9178	24	4	3	4	0.9149	14	3	2	5	0.9095	16	3	6	3
0.9050	18	5	3	3	0.9023	32	0	0	6*M*	0.9023	32	5	5	1*M*
0.8978	19	2	8	0	0.8968	11	6	1	2	0.8955	5	6	3	0
0.8943	6	4	6	2	0.8923	28	0	8	2	0.8856	6	1	1	6
0.8832	15	3	3	5	0.8784	34	6	2	2	0.8634	11	4	7	0
0.8628	18	5	4	3	0.8612	11	2	0	6	0.8557	11	2	1	6
0.8521	26	2	8	2	0.8502	7	6	3	2	0.8407	6	1	3	6
0.8344	28	3	7	3	0.8285	8	1	8	3	0.8256	29	4	5	4
0.8226	35	4	7	2	0.8216	5	1	9	1	0.8166	5	3	0	6
0.8163	25	5	5	3	0.8149	18	2	3	6*M*	0.8149	18	6	4	2*M*
0.8146	28	0	4	6	0.8132	60	1	6	5	0.8119	35	7	0	1
0.8101	16	2	7	4	0.8093	5	6	5	0	0.8063	8	2	9	0
0.8001	30	3	5	5	0.7982	10	3	2	6					

The symbol '*d*' refers to *d*-spacing values; '*I*' refers to *I* integrated intensity value (scaled according to the maximum value of 999; the symbol * indicates the strongest peak); the *h k l* values are the Miller indexes; *M* and + refer to peaks containing contributions from two and more than two reflections, respectively.

Table 7
X-ray reference pattern for Y_2TiCuO_6, $P6_3cm$ (no. 62), $a = 6.18215(4)$ Å, $c = 11.49047(12)$ Å, $V = 380.318(6)$ Å^3.

d (Å)	I	h	k	l	d (Å)	I	h	k	l	d (Å)	I	h	k	l
5.74524	100	0	0	2	5.35390	10	1	0	0	3.91683	20	1	0	2
3.09107	302	1	1	0	2.98495	609	1	1	1	2.87262	373		0	4
2.72210	999*	1	1	2	2.53128	11	1	0	4	2.42648	16	2	0	2
2.40545	23	1	1	3	2.10424	291	1	1	4	1.95841	11	2	0	4
1.90865	8	2	1	2	1.84425	108	1	1	5	1.80319	37	1	0	6
1.78463	496	3	0	0	1.70430	43	3	0	2	1.65433	18	2	1	4
1.62796	218	1	1	6	1.55755	23	2	0	6	1.54554	42	2	2	0
1.53174	49	2	2	1	1.51591	267	3	0	4	1.49248	152	2	2	2
1.44976	43	1	1	7	1.43631	23	0	0	8	1.43325	7	2	2	3
1.39094	22	2	1	6	1.38726	9	1	0	8	1.36105	56	2	2	4
1.30256	11	1	1	8	1.28248	17	2	2	5	1.20272	63	2	2	6
1.17348	14	3	1	6	1.17126	9	2	1	8	1.16832	31	4	1	0
1.16232	23	4	1	1	1.14488	129	4	1	2	1.12526	12	2	2	7
1.12347	9	1	0	10	1.11893	55	3	0	8	1.11749	6	4	1	3
1.08223	53	4	1	4	1.07704	12	1	1	10	1.05589	7	2	0	10
1.05212	8	2	2	8	1.04146	17	4	1	5	1.03389	10	3	2	6
1.03238	9	3	1	8	1.03036	49	3	3	0	1.01418	11	3	3	2
0.99920	19	2	1	10	0.99737	84	4	1	6	0.98961	9	1	1	11
0.96986	49	3	3	4	0.95184	12	4	1	7	0.92212	8	2	2	10
0.90874	12	3	1	10	0.90634	14	4	1	8	0.89461	7	4	2	6
0.89232	37	6	0	0	0.88174	6	6	0	2	0.86553	10	2	1	12
0.85934	6	5	1	6	0.85731	21	5	2	0	0.85493	9	5	2	1
0.85215	52	6	0	4	0.84982	7	1	1	13	0.84792	96	5	2	2
0.84376	28	3	0	12	0.83911	11	3	2	10	0.83722	33	3	3	8
0.82151	55	5	2	4	0.81923	29	4	1	10	0.80473	14	3	1	12
0.80324	14	5	2	5	0.79975	11	4	3	6	0.79905	11	5	1	8

The symbol '*d*' refers to d-spacing values, '*I*' refers to *I* integrated intensity value (scaled according to the maximum value of 999; the symbol * Indicates the strongest peak); the *h k l* values are the Miller indexes; *M* and + refer to peaks containing contributions from two and more than two reflections, respectively.

Acknowledgments

The authors acknowledge the partial financial support from the US Department of Energy and also from International Centre for diffraction Data. Mr. N. Swanson is thanked for his graphical assistance.

References

[1] A.P. Malozemoff, D.T. Verebelyi, S. Fleshler, D. Aized, D. Yu, Physica C 385 (2003) 424–430.
[2] M.W. Rupich, W. Zhang, X. Li, T. Kodenkandath, D.T. Verebelyi, U. Schoop, C. Thieme, M. Teplitsky, J. Lynch, N. Nguyen, E. Siegal, J. Scudiere, V. Maroni, K. Venkataraman, D. Miller, T.G. Holesinger, Physica C 412–414 (2004) 877–884.
[3] A. Goyal, D.P. Norton, J.D. Budai, M. Paranthaman, E.D. Specht, D.M. Kroeger, D.K. Christen, Q. He, B. Saffian, F.A. List, D.F. Lee, P.M. Martin, C.E. Klabunde, E. Hartfield, V.K. Sikka, Appl. Phys. Lett. 69 (1996) 1795–1797.
[4] A. Goyal, U. Schoop, P. Paranthaman, MRS Bull. 29 (2004) 552–563.
[5] P.N. Arendt, S.R. Foltyn, L. Civale, R.F. DePaula, P.C. Dowden, J.R. Groves, T.G. Holesinger, Q.X. Jia, S. Kreiskott, L. Stan, I. Usov, H. Wang, J.Y. Coulter, Physica C 412–414 (2004) 795–800.
[6] S.R. Foltyn, E.J. Peterson, J.Y. Coulter, P.N. Arendt, Q.X. Jia, P.C. Dowden, M.P. Maley, X.D. Wu, D.E. Peterson, J. Mater. Res. 12 (1997) 2941–2946.
[7] Y. Yamada, A. Ibi, H. Fukushima, R. Kuriki, S. Miyata, K. Takahashi, H. Kobayashi, S. Ishida, M. Konishe, T. Kato, T. Hirayama, Y. Shiohara, Physica C 445–448 (2006) 504–508.
[8] R. Feenstra, T.B. Lindemer, J.D. Budai, M.D. Galloway, J. Appl. Phys. 69 (1991) 6569.
[9] V. Selvamanickam, H.G. Lee, Y. Li, X. Xiong, Y. Qiao, J. reeves, Y. Xie, A. Knoll, K. Lenseth, Physica C 392–396 (2003) 859–862.
[10] V. Selvamanickam, Y. Chen, X. Xiong, Y.Y. Xie, J.L. Reeves, X. Zhang, Y. Qiao, K.P. Lenseth, R.M. Schmidt, A. Rar, D.W. Hazelton, K. Tekletsadik, IEEE Trans. Appl. Superconductivity 17 (2) (2007) 3231–3234.
[11] P.M. Mankiewich, J.H. Scofield, W.J. Skocpol, R.E. Howard, A.H. Dayem, E. Good, Appl. Phys. Lett. 51 (21) (1987) 1753.
[12] S.-W. Chan, B.G. Bagley, L.H. Greene, M. Giroud, W.L. Feldmann, K.R. Jenkin II, B.J. Wilkins, Appl. Phys. Lett. 53 (15) (1988) 1443.
[13] P.C. McIntye, M.J. Cima, J. Mater. Res. 9 (9) (1994) 2219.
[14] P.C. McIntyre, M.J. Cima, A. Roshko, J. Appl. Phys. 77 (10) (1995) 5263.
[15] W. Wong-Ng, L.P. Cook, P. Schenck, I. Levin, Z. Yang, Q. Huang, J. Frank, in: Proceedings of the PACRIM meeting, sponsored by ACerS, Maui, Hawaii, September 2005, Ceramic Trans. 191 (2006) 83–98.
[16] L.P. Cook, W. Wong-Ng, P. Schenck, Z. Yang, I. Levin, J. Frank, J. Electron. Mater. 36 (10) (2007) 1293–1298.
[17] W. Wong-Ng, I. Levin, M. Otani, M.D. Vaudin, L.P. Cook, J. Cline, R. Feenstra, T. Holesinger, Appl. Phys. Lett. 90 (2007) 102508.
[18] W. Wong-Ng, I. Levin, L.P. Cook, R. Feenstra, Appl. Phys. Lett 88 (2006) 102507.
[19] W. Wong-Ng, I. Levin, R. Feenstra, L.P. Cook, M. Vaudin, Supercond. Sci. Technol. 17 (2004) S548.
[20] W. Wong-Ng, I. Levin, M. Vaudin, R. Feenstra, L.P. Cook, J.P. Cline, Adv. X-ray Diffr. 46 (2002) 257–263.
[21] PDF, Powder Diffraction File, Produced by ICDD, Newtown Square, 12 Campus Blvd., Newtown Squares PA 19073-3273, USA.
[22] H.M. Rietveld, J. Appl. Cryst. 2 (1969) 65.
[23] A.C. Larson, R.B. von Dreele, (1992). GSAS—General Structure Analysis System, US Government Contract (W-7405-ENG-36) by the Los Alamos National laboratory, which is operated by the University of California for the US Department of Energy.
[24] M.T. Anderson, V.F. Balbarin, D.A. Groenke, G.A. Bain, K.R. Poeppelmeier, J. Solid State Chem. 103 (1993) 216–227.
[25] A.A. Slobodyanyuk, Yu.D. Tret'yakov, A.F. Bessonov, Russ. J. Inorg. Chem. 17 (6) (1972) 922.
[26] D. Hennings, J. Solid State Chem. 31 (1980) 275–279.
[27] M.H. Mueller, H.W. Knott, Trans. Metall. Soc. AIME 227 (1963) 674.
[28] G. Kelkar, A. Carim, J. Am. Ceram. Soc. 76 (1993) 1815.
[29] M. Richard, L. Brohan, M. Tournoux, J. Solid State Chem. 112 (1994) 345–354.
[30] M. Abe, K. Uchino, Mater. Res. Bull. 9 (1974) 147.
[31] A.P. Ramirez, M.A. Subramanian, M. Gardel, G. Blumberg, D. Li, T. Vogt, S.M. Shapiro, Solid State Commun. 115 (2000) 217–220.
[32] M.A. Subramanian, D. Li, N. Duan, B.A. Reisner, A.W. Sleight, J. Solid State Chem. 151 (2000) 323–325.
[33] C.C. Holmes, T. Vogt, S.M. Shapiro, S. Wakimoto, A.P. Ramirez, Science 293 (2001) 27.
[34] X. Shan, X. Yang, K. Zhang, Z. Cheng, Mater. Res. Soc. Symp. Proc. 949 (2007) C05.
[35] W. Wong-Ng, J.A. Kaduk, J. Suh, Powder Diffr. 20 (3) (2005) 193–197.
[36] J. Chenavas, J.C. Joubert, M. Marezio, B. Bochu, J. Solid State Chem. 14 (1975) 25–32.
[37] I. Bryntse, P.-E. Werner, Mater. Res. Bull. 25 (1990) 477–483.
[38] M.N. Deschizeaux, J.C. Joubert, A. Vegas, A. Collomb, J. Chenavas, M. Marezio, J. Solid State Chem. 19 (1976) 45–51.
[39] M.T. Anderson, K.B. Greenwood, G.A. Taylor, K.R. Poeppelmeier, Prog. Solid State Chem. 22 (1993) 197–233.
[40] V.M. Goldschmidt, Str. Nor. Vidensk-Akad. Oslo 1 (1926) 1.
[41] R.D. Shannon, C.T. Prewitt, Acta Crystallogr. 25 (1969) 925–946.
[42] R.D. Shannon, Acta Crystallogr. A 32 (1976) 751–767.
[43] N. Floros, J.T. Rijssenbeek, A.B. Martinson, K.R. Poeppelmeier, Solid State Sci. 4 (2002) 1495–1498.
[44] P. Coppens, M. Eilschuetz, Acta Crystallogr. 19 (1965) 524.
[45] A.M. Glazer, Acta Crystallogr. B 28 (1972) 3384–3392.
[46] I.D. Brown, D. Altermatt, Acta Crystallogr. B 41 (1985) 244–247.
[47] N.E. Brese, M. O'Keeffe, Acta Crystallogr. B 47 (1991) 192.